RESEARCH Open Access



Effect of Blending Silica Fume and GGBS on Chloride Penetration in Concrete under Temperature Gradient Conditions

Remilekun A. Shittu^{1,2}, Akram AlFantazi^{2,3}, Ahmed K. Alkaabi^{2,4} and Tae-Yeon Kim^{1,2*}

Abstract

This paper investigates the significance of thermal diffusion on chloride diffusion in concrete under high ambient temperature in arid climates. Of particular interest is to study the effects of silica fume (SF) and ground granulated blast furnace slag (GGBS) on chloride penetration into concrete subjected to temperature gradient conditions. This was achieved by making three sets of concrete samples—the control samples, the samples containing 5% SF, and the samples containing 5% SF and 50% GGBS. These samples were exposed to a NaCl environment under isothermal and thermal gradient conditions. The total and free chloride contents of the exposed samples were determined via potentiometric titration. The total chloride concentration of the samples exposed to thermal gradient conditions could be 1.3–6 times higher than those exposed to isothermal conditions at the same temperature. The addition of SF and GGBS yielded significantly lower total and free chloride contents than the control samples under isothermal and thermal gradient conditions. While thermal gradient significantly reduces the chloride binding capacity, adding SF and GGBS increases this ability. SEM analysis revealed microstructural changes in concrete due to high temperature and thermal gradients, with larger and deeper pores in samples exposed to thermal gradient. Numerical estimation of chloride concentration and the corrosion initiation time of a reactor containment building was also performed using the modified chloride diffusion equation, including the effects of mass- and thermo-diffusion.

Keywords Temperature gradient, Chloride diffusion, Soret effect, Ambient temperature, Chloride binding capacity, Fick's law

Journal information: ISSN 1976-0485 / eISSN 2234-1315.

*Correspondence:

Tae-Yeon Kim

taeyeon.kim@ku.ac.ae

- ¹ Civil and Environmental Engineering, Khalifa University of Science and Technology, Abu Dhabi 127788, UAE
- ² Emirates Nuclear Technology Centre, Khalifa University of Science and Technology, Abu Dhabi 127788, UAE
- ³ Chemical Engineering, Khalifa University of Science and Technology, Abu Dhabi 127788, UAE
- ⁴ Mechanical and Nuclear Engineering, Khalifa University of Science and Technology, Abu Dhabi 127788, UAE

1 Introduction

Chloride diffusion in concrete structures is a major durability issue. Chloride ions can penetrate the permeable concrete matrix and reach the reinforcing steel bars, corrode them, and reduce the lifespan of the structures (Bolzoni et al., 2021; Tian, et al., 2023). The diffusion of chloride ions into concrete structures is primarily influenced by two factors—concrete properties, such as porosity, permeability, chloride binding capacity, and cracks; and environmental factors, such as temperature and relative humidity (Gjørv, 2011). The durability of concrete structures could be enhanced by optimizing the concrete mix proportions, using additives, supplementary cementitious materials (SCMs), macro- and nanoparticles, etc. Specifically, SCMs such as fly ash (FA),



© The Author(s) 2025. **Open Access** This article is licensed under a Creative Commons Attribution-NonCommercial-NoDerivatives 4.0 International License, which permits any non-commercial use, sharing, distribution and reproduction in any medium or format, as long as you give appropriate credit to the original author(s) and the source, provide a link to the Creative Commons licence, and indicate if you modified the licensed material. You do not have permission under this licence to share adapted material derived from this article or parts of it. The images or other third party material in this article are included in the article's Creative Commons licence, unless indicated otherwise in a credit line to the material. If material is not included in the article's Creative Commons licence and your intended use is not permitted by statutory regulation or exceeds the permitted use, you will need to obtain permission directly from the copyright holder. To view a copy of this licence, visit https://creativecommons.org/licenses/by-nc-nd/4.0/.

Shittu et al. Int J Concr Struct Mater (2025) 19:54 Page 2 of 19

SF, GGBS, limestone powder, and metakaolin have been widely reported to reduce chloride diffusion in concrete. This is because they can reduce porosity, inhibit chloride diffusion, enhance chemical stability, reduce chloride diffusion coefficient, and ultimately improve the service life of concrete structures (Al-Sodani, 2022a; Basha et al., 2020; Bolzoni et al., 2021; Criado et al., 2018; Luo et al., 2003; Zhang et al., 2017). Although the use of SCMs in concrete for arid climates has been extensively studied, the impact of thermal gradients remains unexplored. This study is to examine the influence of SCMs, in particular, SF and GGBS, on chloride diffusion in concrete subjected to the thermal gradient condition at high ambient temperature in arid climate regions.

Many studies have verified the effects of SF and GGBS on chloride diffusion in concrete subjected to isothermal conditions. For example, in an experimental work by Zhang et al., (2017), concrete samples containing different SCMs such as basalt fiber, FA, and SF were exposed to 12.5% NaCl for up to 400 days at room temperature. They observed that the concrete specimens incorporated with 5% SF by weight of concrete had the least porosity. In another experimental study (Al-Sodani, 2022a), SF was used as a replacement of cement at 5%-15% by weight. Concrete specimens were exposed to chloride environment at different isothermal temperatures, i.e., 23, 38, 53, and 68 °C. They reported that the apparent diffusion coefficient of concrete containing SF could reduce by 1.4–7.3 times compared to the reference concrete sample and increase as temperature rises. Similarly, GGBS has also been used to inhibit chloride diffusion in concrete. In a study by Basha et al., (2020), the addition of GGBS reduces the permeability of chloride ion into concrete especially at higher replacement percentages. In addition to the enhancement of the calcium silicate hydrate (CSH) gel formation, GGBS helps in refining the concrete pores and improve the chloride binding capacity of concrete due to the formation of stable salt, such as the Friedel's salt (Luo et al., 2003). Furthermore, because of its fineness, GGBS can reduce the porosity of concrete and aid the formation of a passive layer on steel reinforcement bars (Criado et al., 2018). Further research works on the impact of elevated temperatures on chloride penetration into concrete in arid environments is available in references (Al-Sodani et al., 2021; Al-Sodani, 2022b; de Assis Oliveira et al., 2024). Al-Sodani (2022b) investigated the exposure of concrete containing SF and metakaolin to chloride solutions at temperatures of 23, 38, 53, and 68 °C. They found that SF-containing samples exhibited a 1.4-7.3 times lower chloride diffusion coefficient compared to OPC concrete. In an earlier study (Al-Sodani et al., 2021), fly ash concrete was exposed to chloride environments at 22, 35, 50, and 60 °C for 365 days in laboratory conditions, while beams were subjected to tidal zones for 10 years. The study concluded that FA improved chloride resistance in both conditions compared to OPC concrete. de Assis Oliveira et al. (2024) examined chloride penetration in fire-damaged concrete by subjecting it to temperatures of 25, 200, 500, and 700 °C while also assessing the impact of different cooling methods. Their findings indicated that GGBS concrete effectively reduced crack propagation and chloride penetration at 500 and 700 °C, but showed no significant advantage at 200 °C. In all these studies, the exposure temperatures were maintained under isothermal conditions.

Meanwhile, in arid climates, the development of temperature gradient in concrete structures influenced by high environmental temperatures could accelerate chloride ion diffusion. In our previous study (An et al., 2022), it was concluded that thermal diffusion—the movement of chloride ions due to temperature gradient-significantly increases chloride diffusion in concrete. Specifically, chloride concentrations in temperature gradient conditions can range from 1.33 to 3.30 times higher than those in isothermal conditions at 50 °C ambient temperature. In another work, Isteita and Xi (2017) conducted an experimental study on the effect of temperature variation on chloride ion diffusion in concrete. According to their findings, there is a significant increase in chloride ion diffusion if temperature and chloride concentration gradients are in the same direction. Bai et al. (2019) developed an analytical solution for predicting chloride transport in concrete considering temperature gradient. Consequently, in arid regions, where concrete structures are at proximity to seawater, these structures can be subjected to increased chloride ion diffusion due to the combination of temperature and chloride concentration gradients. The phenomenon responsible for the increased diffusion is termed thermal or thermo-diffusion or Soret effect. None of the previous studies considered the effects of SF and GGBS on chloride ion diffusion due to thermal diffusion in arid climate conditions in depth.

Although the effectiveness of SCMs such as SF and GGBS in preventing chloride diffusion in concrete has been extensively examined, all the earlier works considered exposure of concrete to chloride environments in isothermal conditions. To the best of our knowledge, this is the first study to investigate the influence of SF and GGBS on chloride ion diffusion in concrete under the temperature gradient conditions. In arid climates such as the Arabian Gulf region, SF and GGBS are frequently added to concrete to decrease permeability and address thermal cracking, which is prevalent due to the high ambient temperatures experienced in summer (Ahmad et al., 2022; Arivalagan, 2014; Jagan & Neelakantan, 2021; Sothornchaiwit

Shittu et al. Int J Concr Struct Mater (2025) 19:54 Page 3 of 19

et al., 2022; Zhao et al., 2020). Arivalagan (2014) and Ahmad et al. (2022) concluded that incorporating SF and GGBS into concrete enhances its mechanical properties and durability, particularly in hot climates. Similarly, Zhao et al. (2020) conducted a study simulating concrete with GGBS exposed to a chloride-rich submerged environment and concluded that at higher replacement percentages, the addition of GGBS enhances chloride inhibition when compared to ordinary Portland cement concrete. Jagan and Neelakantan (2021) found that replacing 15% of cement with SF provided the highest resistance to acid attack. They also reported improved compressive strength and increased shrinkage resistance with higher SF content. Meanwhile, another study (Sothornchaiwit et al., 2022) identified an optimal 6% SF replacement for achieving the highest sulfate resistance in concrete cured in sulfate solution at 30, 45, and 60 °C. Hence the justification of using SF and GGBS in this study (Elchalakani et al., 2014). Moreover, as established in prior research (An et al., 2022; Bai et al., 2019; Isteita & Xi, 2017), thermal diffusion expedites the ingress of chloride ions into concrete, a phenomenon that can be ameliorated by incorporating SCMs, such as SF and GGBS. Nevertheless, the magnitude of their mitigating influence and their efficacy in concrete exposed to thermal diffusion are yet to be investigated. As such, the following questions arise: are SF and GGBS capable of offsetting the additional chloride ion content in concrete structures induced by thermal diffusion? What is the impact of thermal diffusion on chloride binding capacity of concrete? What is the impact of SF and GGBS on the overall service life of concrete structures in arid climate regions? The objective of this study is to provide answers to such questions via experimental and numerical works. The novelty of this research lies in exploring how blended cementitious materials, such as silica fume (SF) and ground granulated blast furnace slag (GGBS), mitigate chloride penetration under thermal gradient conditions and whether these supplementary cementitious materials (SCMs) can reduce the impact of accelerated chloride ingress caused by thermal diffusion. It also involves examining chloride penetration and the corrosion initiation time of blended cement concrete under the influence of thermal diffusion.

For the experimental work, the concrete samples including SF and GGBS in addition to cement along with the control samples without SF and GGBS are produced. Chloride diffusion tests are performed using the concrete samples at three different exposure scenarios, i.e., two isothermals at 22 and 50 °C and one temperature gradient at 50 °C. The total and free chloride contents over the depth of concrete are then measured by potentiometric titration. The effects of SF and GGBS on the chloride binding capacity under the temperature gradient condition are evaluated using the measured total and free chlorides. Scanning

electron microscopy (SEM) is used to analyze the microstructural changes in concrete samples after exposure to the different chloride environments. For numerical work, finite element analysis of chloride diffusion in concrete due to thermal diffusion is preformed using the modified chloride diffusion equation including both spatial variation of temperature in mass diffusion and temperature gradient in thermal diffusion. Numerical results are verified by comparing with experimental data and the corrosion initiation time of a reactor containment building (RCB) in nuclear power plant situated in arid climate is numerically predicted for various temperature gradient conditions.

The remainder of the paper is organized as follows. In Sect. 2, the preparation of the concrete samples along with the characterization of the materials is presented. The experimental methodology used in this study is extensively discussed in Sect. 3. The results of the experiments as well as those of the numerical simulations are reported in Sect. 4. Finally, the conclusion and summary of this study are provided in Sect. 5.

2 Sample Preparation

2.1 Material Characterization

The cement used for this study is type 1 ordinary Portland cement and SF (Sigma-Aldrich®) has a size of $0.2-0.3 \ \mu m$. The X-ray powder diffraction (XRD) technique was carried out on cement, SF, and GGBS. X-rays were directed at the samples and the angles at which X-rays are diffracted (2 θ) are referred to as the diffraction angle. Figure 1 shows XRD images for these three binders. It was observed that GGBS and SF have only one broad peak at an angle of 30° and 15°, respectively. While cement has multiple sharp peaks with the highest peak obtained at a diffraction angle of 32°. These peak patterns are similar to what has been reported in previous studies (see, for example, Nguyen et al., 2016; Tanu & Unnikrishnan, 2023; Iqbal et al., 2022), for XRD images on cement, GGBS, and SF, respectively. By comparing the peak pattern with a database of chemicals with known XRD peak patterns, it was determined that the multiple peaks in the cement samples include a combination of Alite (Ca₃SiO₅) corresponding to JCPDS 49-0442, Belite (Ca₂SiO₄) with JCPDS 33-0302, tricalcium aluminate (C₃A) with JCPDS 38-1429, and tetraaluminoferrite (C₄AF) with JCPDS 40-0218 card numbers. These compounds influence the hydration reaction of cement with water. Meanwhile, the broad peak for GGBS correlates mostly with JCPDS 35-0610 which is the crystalline phase of GGBS (Reshma et al., 2023; Tanu & Unnikrishnan, 2023). Finally, for the SF sample, the peak majorly signifies the presence of silica (SiO₂) which correlates with JCPDS 46-1045 card number.

Shittu et al. Int J Concr Struct Mater (2025) 19:54 Page 4 of 19

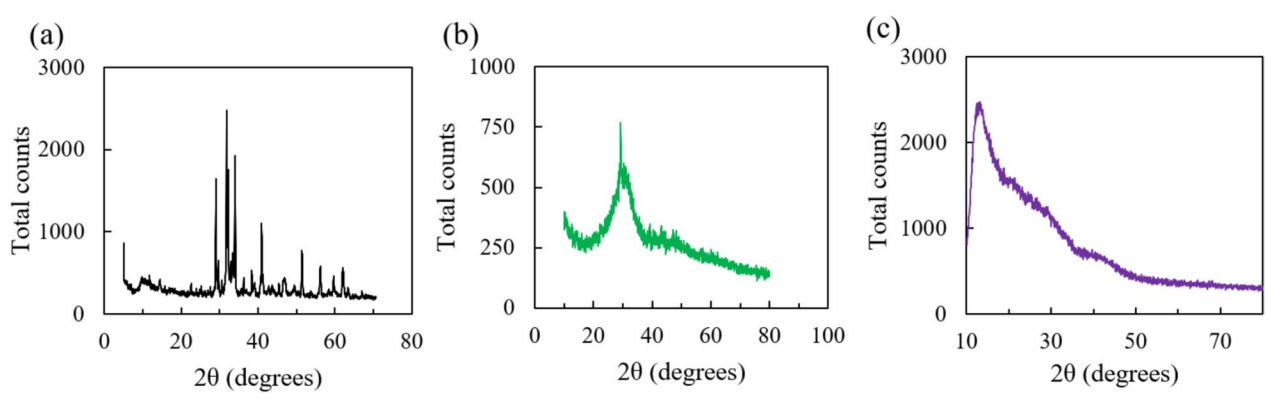


Fig. 1 X-ray diffraction images for the three binders: a Cement, b GGBS, and c SF

Table 1 Chemical compositions and physical properties of the materials

Chemical co	omposition	(%)							
Material	C ₃ S	C ₃ A		SO ₃	MgO	Na ₂ O + K ₂ O	Insoluble residual	LOI	Moisture
Cement	70.1	7.42		2.1	1.35	0.62	0.62	1.5	-
	SiO ₂	CaO	Al_2O_3	SO_3	S	Total alkalis	Slag activity (7 days)	LOI	Moisture
SF	86	-		-	0.76	2.4	124	3.7	0.3
GGBS	35	40	15	0.3	-	0.44	86	0.8	-
Physical pro	operties								
Material			Density (g/	′cm³)		Grain siz	ze (cm²/g)		Specific surface (m²/g)
Cement			3.12			3600			-
SF			2.16			=			23.9
GGBS			2.86			4800			-

In Table 1, the physical and chemical properties of the cementitious materials are presented.

The aggregates used for preparing the concrete samples are dune sand, crushed sand, and granite. The physical properties of these aggregates are displayed in Table 2, while Fig. 2 shows the particle size distribution of these aggregates.

From the results, 95% of the dune sand passed through the 0.3 mm sieve while for the fine sand, 97% of the particles passed through the 5 mm sieve. In addition, 30% of the sand passed through the 1 mm sieve. Furthermore, the 20 mm coarse aggregate has 5% passing through the 10 mm sieve, while 94% of the 10 mm coarse aggregate passed through the 10 mm sieve.

2.2 Mix Design of the Concrete Samples

The concrete mix design used for this study is presented in Table 3. A constant water-to-binder ratio was used throughout the study to solely identify the effects of SF

Table 2 Physical properties of aggregates

Aggregates	Specific gravity	Absorption (%)		
Crushed sand	2.69	1.2		
Dune sand	2.63	0.7		
Coarse aggregate	2.69	0.6		

and GGBS on the chloride ion diffusion in concrete. Thirty-three cylindrical concrete samples of approximately 80 mm height and 96 mm diameter were cast and cured for 28 days as detailed in Table 4. These concrete samples consist of the control (CT) samples containing only ordinary Portland cement as a binder, the samples containing 5% SF, called the SF samples, and the samples containing 5% SF and 50% GGBS, called the SF+GGBS samples. Twenty-one samples were used for chloride

Shittu et al. Int J Concr Struct Mater (2025) 19:54 Page 5 of 19

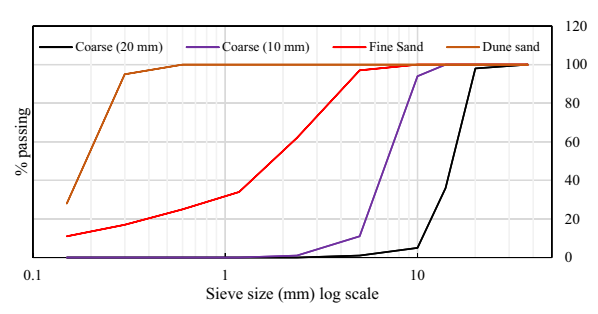


Fig. 2 Sieve analysis of the aggregates showing the percentages of each aggregate that pass through different sieve sizes

Table 3 Mix proportions of the CT, SF, and SF + GGBS samples

Component	СТ	SF	SF+GGBS
Water (kg/m ³)	255.74	266.34	266.34
Water-to-binder ratio	0.65	0.65	0.65
Cement (kg/m³)	393.44	390.24	195.12
Silica fume (kg/m³)	-	19.51	19.51
GGBS (kg/m³)	-	-	195.12
Aggregate-binder ratio	4.5	4.5	4.5
Dune sand (kg/m³)	590.16	585.36	585.36
Fine aggregate (crushed sand) (kg/m³)	590.16	585.36	585.36
Coarse aggregate (d \leq 20 mm) (kg/m ³)	590.16	585.36	585.36

Table 4 Quantity and dimensions of concrete samples

Sample type	Number of samples	Dimension		
CT	11	Height: 80 mm		
SF	11	Diameter: 96 mm		
SF+GGBS	11			
Total	33			
iOtai	33			

diffusion tests and 12 samples were used for the porosity measurement.

3 Methodology

The chloride diffusion tests were conducted by exposing three types of samples (i.e., CT, SF, and SF+GGBS sample) to chloride environments at three different temperature conditions: isothermal temperature of 22 °C (IT22), isothermal temperature of 50 °C (IT50), and temperature gradient (TG) caused by the ambient temperature of 50 °C. The experimental setups for these three chloride environments are described in Sect. 3.1.

3.1 Experimental Setup

Figure 3 shows the experimental setups established for chloride diffusion tests in both isothermal and temperature gradient conditions.

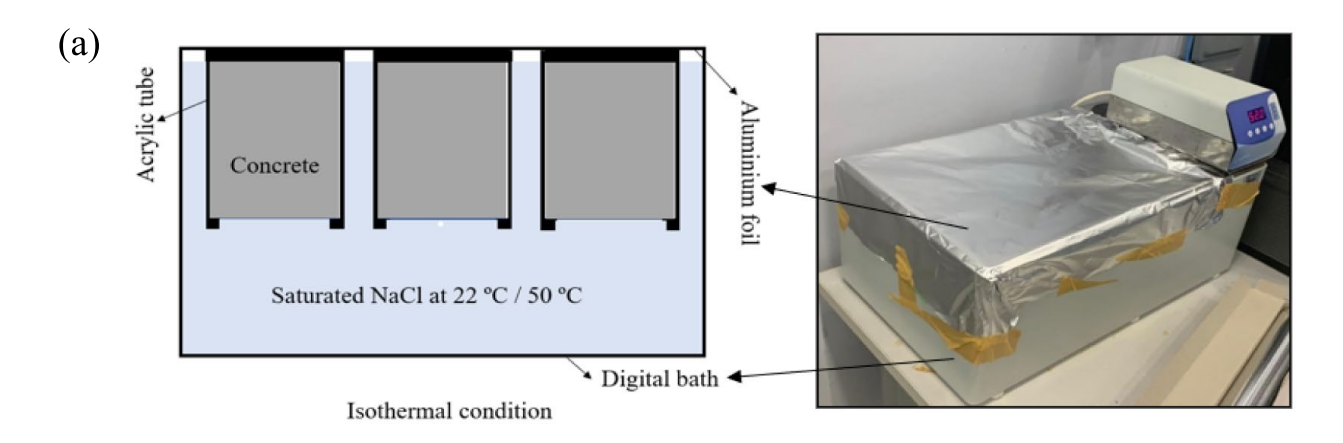
The concrete samples were exposed to chloride environments under a fully saturated pore condition for 30 days. For the isothermal condition, they were totally immersed in the saturated NaCl solution at temperatures of 22 °C (IT22) and 50 °C (IT50), as shown in Fig. 3a. For the temperature gradient (TG) condition, only the exposed surface is in contact with the heated NaCl solution at 50 °C, and the other end subjected to air cooling at room temperature to maximize temperature gradient, as shown in Fig. 3b. Notice that the concrete samples were inserted into acrylic tubes to ensure that chloride ions diffused through the depth in one direction. The pH of the NaCl solution at 22 °C was approximately 7.05 ± 0.10 , while the pH of the solution at 50 °C was between 6.70 ± 0.15 throughout the test. Thermocouples were inserted at three depths, i.e., 10-, 40-, and 70 mm, to measure the temperature variation over the depth of concrete during the period of the test.

3.2 Total and Free Chloride Content Measurement

Sequel to the exposure of the concrete samples to the chloride ion environment for 30 days, the samples were then prepared for potentiometric titration by cutting six 10 mm slices of concrete to profile the chloride concentration at every 10 mm depth. The slices are then pulverized into powder that pass through the 850 µm sieve. Both total and free chloride contents were measured in accordance with the provisions of ASTM C1152/C1152M-20 (ASTMC642-06, 2006) and ASTM C1218/C1218M-17 (ASTM, 2012a), respectively.

For the total or acid-soluble chloride content measurement, approximately 10 g of the pulverized concrete powder was measured and poured into a 250 ml glass beaker. This powder was dispersed with 75 ml of deionized water and stirred. Thereafter, 50 ml of dilute (1+1)nitric acid (HNO₃) was added to the solution. The dilute HNO₃ extracts the bound chloride ion from the concrete. A few drops of methyl orange indicator were added to the solution and stirred. It was noticed that the color of the indicator changed to red which indicated the acidity of the solution. The resulting solution was heated to boil and allowed to cool. Thereafter, 5 ml of 0.05 N NaCl was added to the cooled solution. Finally, the solution was titrated against standard solution (0.05 N) of Silver Nitrate (AgNO₃) using the Gamry® open circuit potential with AgCl-coated Ag billet electrode as the working electrode and saturated calomel electrode as a reference electrode. The volume of AgNO₃ consumed when the

Shittu et al. Int J Concr Struct Mater (2025) 19:54 Page 6 of 19



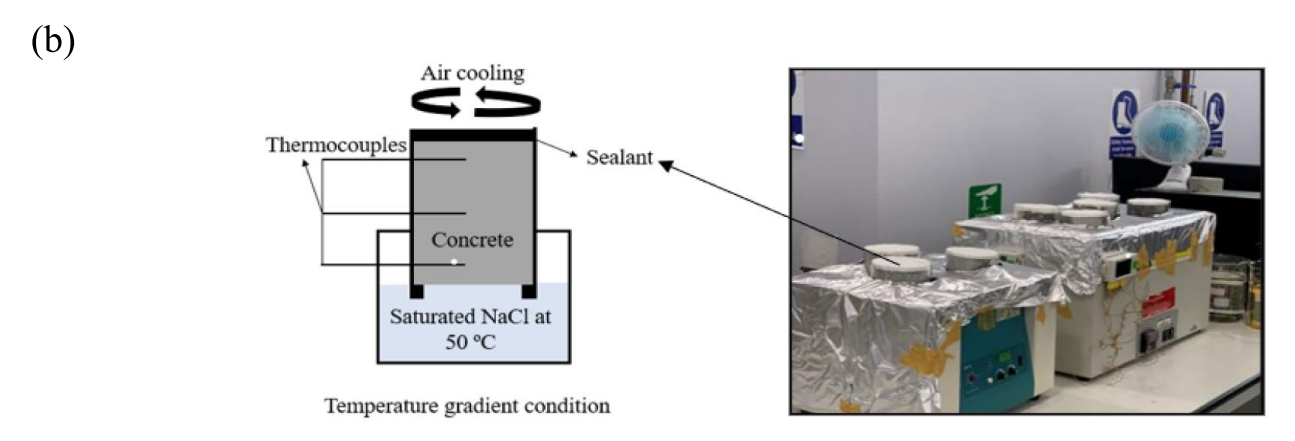


Fig. 3 Experimental setups for the chloride diffusion tests: **a** isothermal condition at 22 $^{\circ}$ C (IT22) and 50 $^{\circ}$ C (IT50) and **b** temperature gradient (TG) condition. Samples exposed to IT22 and IT50 conditions are fully immersed in the NaCl solution, while those samples exposed to TG condition are partially immersed in the NaCl solution with the exposed surface just in contact with the NaCl solution. Thermocouples were inserted at 10-, 40-, and 70 mm depths from the bottom of the concrete samples to record temperature through the depth

equivalent point is reached was recorded. The chloride concentration content was calculated using:

the equipment was calibrated using a standard chloride solution of known concentration, verifying its precision.

$$[C] = \frac{\text{Volume}(\text{AgNO}_3) \times \text{Normality}(\text{AgNO}_3) \times \text{Molarity(chlorine)}}{\text{Mass of concrete}}$$
(1)

where *C* is the chloride ion concentration (wt.% of concrete) and molarity of chlorine is 35.5 g/mol.

For the free or water-soluble chloride measurement, a similar procedure to total chloride measurement was executed. The differences between the procedures are that in the case of free chloride content measurement: (1) dilute ${\rm HNO_3}$ acid was not added to the dispersed concrete powder; (2) after heating to boil, the solution was allowed to cool for 24 h; (3) the solution was filtered through Type II, class G filter paper and only the filtrate was used for the potentiometric titration. The free chloride content was also calculated using Eq. (1). To ensure the accuracy and reliability of potentiometric titration,

The weighing balance used for sample mass measurement has a precision of $\pm\,0.0001$ g. The Gamry potentiostat can detect voltages as low as 1 μV . To maintain the integrity of the pulverized samples, glazed paper was used during pulverization to prevent particle adhesion and minimize contamination or cross-contamination between samples. To minimize errors during titration, the positions of both electrodes were maintained consistently across all measurements, and the temperature was kept stable throughout the process. In addition, an automatic stirrer was used to stir the solution during titration to ensure that the chloride ions were accurately detected. In addition, each sample type was tested in triplicate, and

Shittu et al. Int J Concr Struct Mater (2025) 19:54 Page 7 of 19

the standard deviation (error bars) is presented in the chloride profiles (see Figs. 5–8, 12).

4 Results and Discussion

4.1 Porosity and Temperature Distribution

The porosity of the concrete samples was determined according to the specification of ASTM C642 boiling-water saturation technique (ASTM, 2012b). Twelve cylindrical concrete samples, four samples per sample type, were dried at a temperature range of $100 < T < 110^{\circ} \text{C}$, and cooled in dry air to determine the oven-dry mass. Thereafter, the samples were boiled in distilled water for 5 h and allowed to cool for 19 h to 20 °C to determine the saturated mass. The porosity is then calculated by

Porosity =
$$\frac{m_s - m_d}{m_s - m_b} \times 100\%$$
 (2)

where $m_{\rm s}$ is the saturated surface-dry mass of the specimen in air, $m_{\rm d}$ is the oven-dry mass of the specimen in air, and $m_{\rm b}$ is the buoyant mass of the saturated specimen in water.

Porosities for the CT, SF, and SF+GGBS samples are listed in Table 5. The porosity in the CT sample is relatively larger than that in the SF and SF+GGBS samples. There is an 18% and 23% reduction in porosity in the SF and SF+GGBS samples, respectively, compared to the CT sample. Meanwhile, SF, due to its smaller size

Table 5 Porosity of the CT, SF, and SF + GGBS samples

	СТ	SF	SF+GGBS
Porosity (%)	12.25	10.5	9.48

relative to cement, has been reported to reduce porosity and permeability of concrete because of its ability to refine concrete pores (Shelote et al., 2023). Specifically, SF fills void between cement and aggregates and also reacts with Calcium hydroxide (Ca(OH)₂) in the presence of water to form Ca(OH)₂ gel which fills concrete pores thereby enhancing concrete durability (Vijayan et al., 2023). Similarly, in a study by Huynh et al. (2022), adding dune sand and GGBS to concrete reduced the porosity and enhanced the durability in concrete. GGBS is usually introduced to concrete in high percentages (50% of binder in our case). As a result, they increase the quantity of fines in concrete which results in improved particle packing in concrete in addition to increased formation of CSH gel.

As illustrated in Fig. 3, temperature variations for the CT, SF, and SF + GGBS samples over the 30-day duration were recorded at 10-, 40-, and 70 mm depths under the temperature gradient condition. In Fig. 4a, the temperature recorded at 10- and 70 mm is displayed as a function of time. The temperature reached a steady state after 2 days with minor fluctuations continuing for the following 28 days. The temperature profiles averaged over time throughout the depth of concrete for the CT, SF, and SF+GGBS samples are presented in Fig. 4b. The plots clearly show the presence of temperature gradient within concrete for all the samples under the temperature gradient condition. According to the results, temperature gradients vary in the range of 1.35-1.75 °C/cm depth. Moreover, the temperature variations over depth, i.e., T(x), for all three sample types were obtained by linear fitting of the experimental data. These profiles are used for the numerical estimation of the chloride concentration and the corrosion initiation time in Sect. 5.

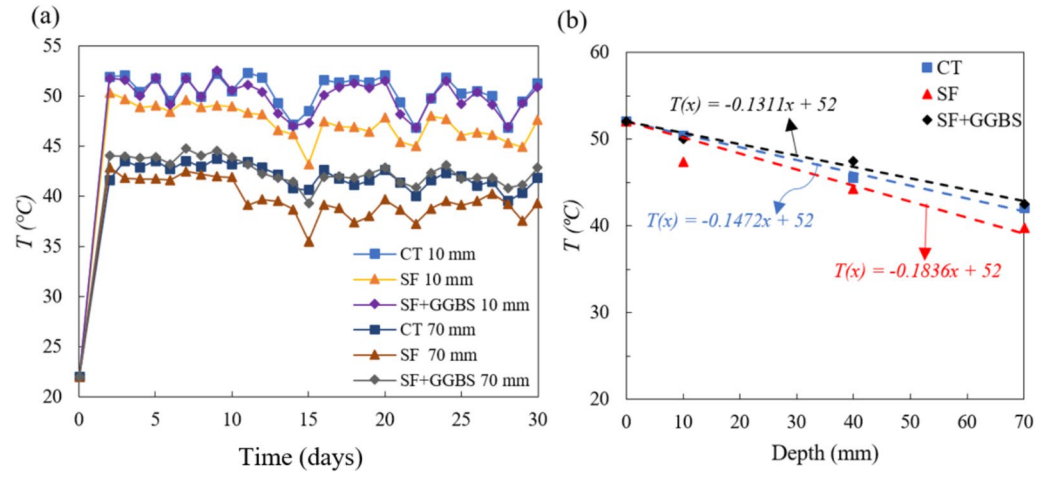


Fig. 4 Measured temperature for 30 days under the temperature gradient condition: **a** Temperature variation over time at the depths of 10 and 70 mm and **b** Time averaged temperature over the depth of concrete along with the linear fitting T(x)

Shittu et al. Int J Concr Struct Mater (2025) 19:54 Page 8 of 19

4.2 Total Chloride Ion Concentration

The total (or acid-soluble) chloride contents in the concrete samples exposed to I22, I50, and TG conditions were measured using potentiometric titration. Two samples were tested for IT22 and IT50 exposure conditions, while three samples were tested for the TG exposure condition. The total chloride ion content was measured at six depths, i.e., 10, 20, 30, 40, 50, and 60 mm, respectively. For each sample type, three samples were used to average total chloride ion contents, which are shown in Table 6.

Using the values in Table 6, the effects of temperature and temperature gradient on total chloride concentration over the depth of concrete are graphically displayed for the CT, SF, and SF+GGBS samples in Fig. 5.

Under isothermal conditions, chloride concentrations for all the three sample sets increase as temperature rises from 22 to 50 °C. This is caused by the enhanced diffusion of chloride ion in these samples because of temperature increase, as described by Fick's law. In contrast to the SF and SF+GGBS samples, the increase in chloride concentration in the CT samples caused by a rise in temperature is more discernible across the depth of concrete. Chloride concentration increases even more under the

TG condition for all three sets of concrete samples. This is due to thermal diffusion or Soret effect as reported in previous studies (An et al., 2022; Bai et al., 2019). According to the results, the average total chloride concentration at the TG condition could be up to 1.3–6 times that at the IT50 condition, indicating the significant effect of temperature gradient on chloride ion penetration into concrete.

In Fig. 6, the effects of SF and GGBS on chloride concentration over depth are examined at three exposure conditions. In comparison with the CT samples, the chloride ion concentration through the depth of concrete is much lower with the addition of SF and GGBS. This trend is consistent for all three exposure conditions due to the reduction in porosity in the SF and SF+GGBS samples. Under the IT22 condition, a 31%–84% reduction in chloride ion content could be attained for the SF samples when compared to the CT samples. This reduction could be up to 35%–93% in the case of the SF+GGBS samples. Under the IT50 condition, there could be up to 40%–88% reduction in the total chloride ion content in the SF samples relative to the CT samples, whereas this reduction could be up to 49%–95% in the SF+GGBS

Table 6 Average total chloride ion content (wt.%) for the CT, SF, and SF + GGBS samples exposed to IT22, IT50, and TG conditions for 30 days

Depth (mm)	СТ			SF	SF			SF + GGBS		
	IT22	IT50	TG	IT22	IT50	TG	IT22	IT50	TG	
10	0.4238	0.8977	1.0178	0.2915	0.5409	0.8871	0.2760	0.4613	0.7272	
20	0.2379	0.7286	0.9247	0.1598	0.3958	0.7099	0.0815	0.2609	0.6260	
30	0.1865	0.5333	0.8163	0.1223	0.2477	0.5652	0.0464	0.1109	0.5017	
40	0.1401	0.4287	0.6258	0.0511	0.0626	0.4115	0.0298	0.0384	0.3361	
50	0.1017	0.3142	0.4614	0.0289	0.0376	0.2946	0.0068	0.0244	0.2025	
60	0.0745	0.2677	0.3239	0.0117	0.0312	0.2508	0.0049	0.0146	0.1560	

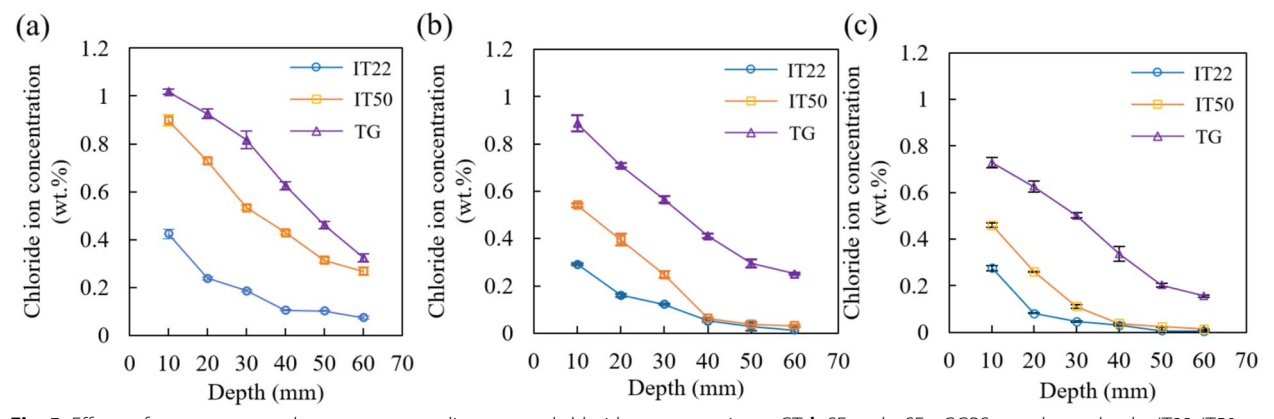


Fig. 5 Effects of temperature and temperature gradient on total chloride concentration: **a** CT, **b** SF, and **c** SF + GGBS samples under the IT22, IT50, and TG conditions

Shittu et al. Int J Concr Struct Mater (2025) 19:54 Page 9 of 19

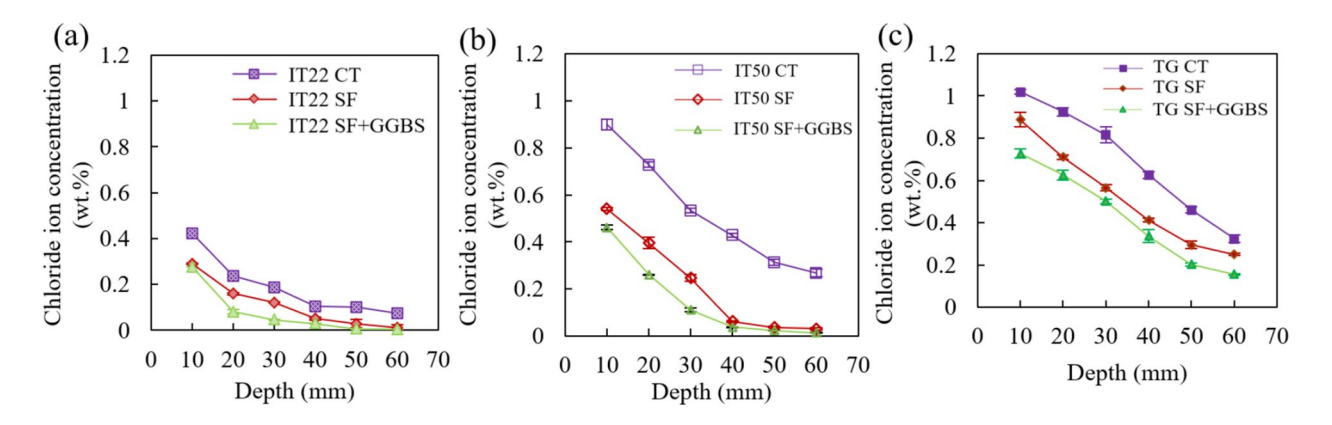


Fig. 6 Effects of SF and GGBS on total chloride concentration under a IT22, b IT50, and c TG exposure conditions

samples. This affirms the ability of SF and GGBS to resist chloride ion diffusion even at isothermal conditions. As shown in Fig. 6a, b, the acid-soluble chloride ion content for the SF+GGBS samples at the IT50 condition is lower than that of the CT samples at the IT22 condition. This demonstrates the ability of SF and GGBS to mitigate chloride ion diffusion caused by a rise in temperature.

Similarly, under the TG condition, there could be 13%-36% and 29%-56% reduction in the total chloride content in the SF and SF+GGBS samples, respectively, when compared to the CT samples. Notice that the inclusion of 5% SF yielded a reduction in the total chloride ion content at the TG condition that is almost equivalent to the chloride content in the CT samples at the IT50 condition as shown in Table 4. Meanwhile, the addition of 5% SF and 50% GGBS could lower the total chloride ion content at the TG condition of the SF+GGBS samples below the IT50 levels of the CT samples. This implies that the addition of SF and GGBS at the proportions demonstrated in this study is effective in offsetting the additional chloride ion content induced by thermal diffusion in the CT samples. This is because both SF and GGBS contain silica (SiO₂), which reacts with calcium hydroxide (Ca(OH)₂), a byproduct of cement hydration, to form C-S-H gel. In addition, GGBS contains CaO and Al₂O₃, which react with water to generate more C-S-H and calcium-aluminate-hydrates (C-A-H), further densifying the mortar matrix and obstructing chloride transport pathways in concrete (see Fig. 7). Chemically, GGBS also interacts with chloride ions to form Friedel's salt (Ca₂Al (OH)₆Cl·2H₂O), a bound form of chloride. Under TG conditions, thermal gradient enhance the movement of moisture and ions, leading to an increased chloride concentration, whereas in isothermal condition, chloride penetration is solely driven by chloride concentration gradient (Kumaran, 1987; Qin & Belarbi, 2005). In contrast, under isothermal conditions, the hydration rates of SF and GGBS remain uniform, resulting in consistent pore refinement. However, in TG conditions, differential hydration rates cause variations in pore structure and permeability, which can enhance chloride ingress. In addition, in isothermal conditions, chloride penetration primarily occurs through diffusion. Under TG conditions, convection effects become more pronounced alongside diffusion, further accelerating chloride transport in blended cement concrete exposed to TG condition (Dehwah & Xi, 2024).

The SEM images of the CT samples reveal the presence of microcracks (Fig. 7a). These microcracks are absent in the SF+GGBS samples (see Fig. 7c). Plate-like calcium hydroxide (CH) crystals are prominent in this CT sample, signifying by-products of cement hydration, which contribute less to the strength and durability of concrete compared to calcium—aluminate—hydrates (C–A–H) or calcium—silicate—hydrates (C–S–H). C–S–H is also visible, but it is less dense.

In the energy dispersive spectroscopy (EDS) images (Figs. 7b, d), the CT samples in Fig. 7b show a higher peak for calcium and oxygen, indicating a significant presence of Ca(OH)₂. However, in Fig. 7d, the lower calcium peak is due to the pozzolanic reaction of SF and GGBS, which forms C–S–H and C–A–H with bound calcium that is less detectable by EDS. In addition, the Ca/Si ratio is lower in the SF+GGBS samples due to the formation of secondary hydration products, such as C–S–H and C–A–H, which offer better resistance to chemical attacks.

4.3 Free Chloride Ion Concentration

The free (or water-soluble) chloride ion contents for the CT, SF, and SF+GGBS samples were measured Shittu et al. Int J Concr Struct Mater (2025) 19:54 Page 10 of 19

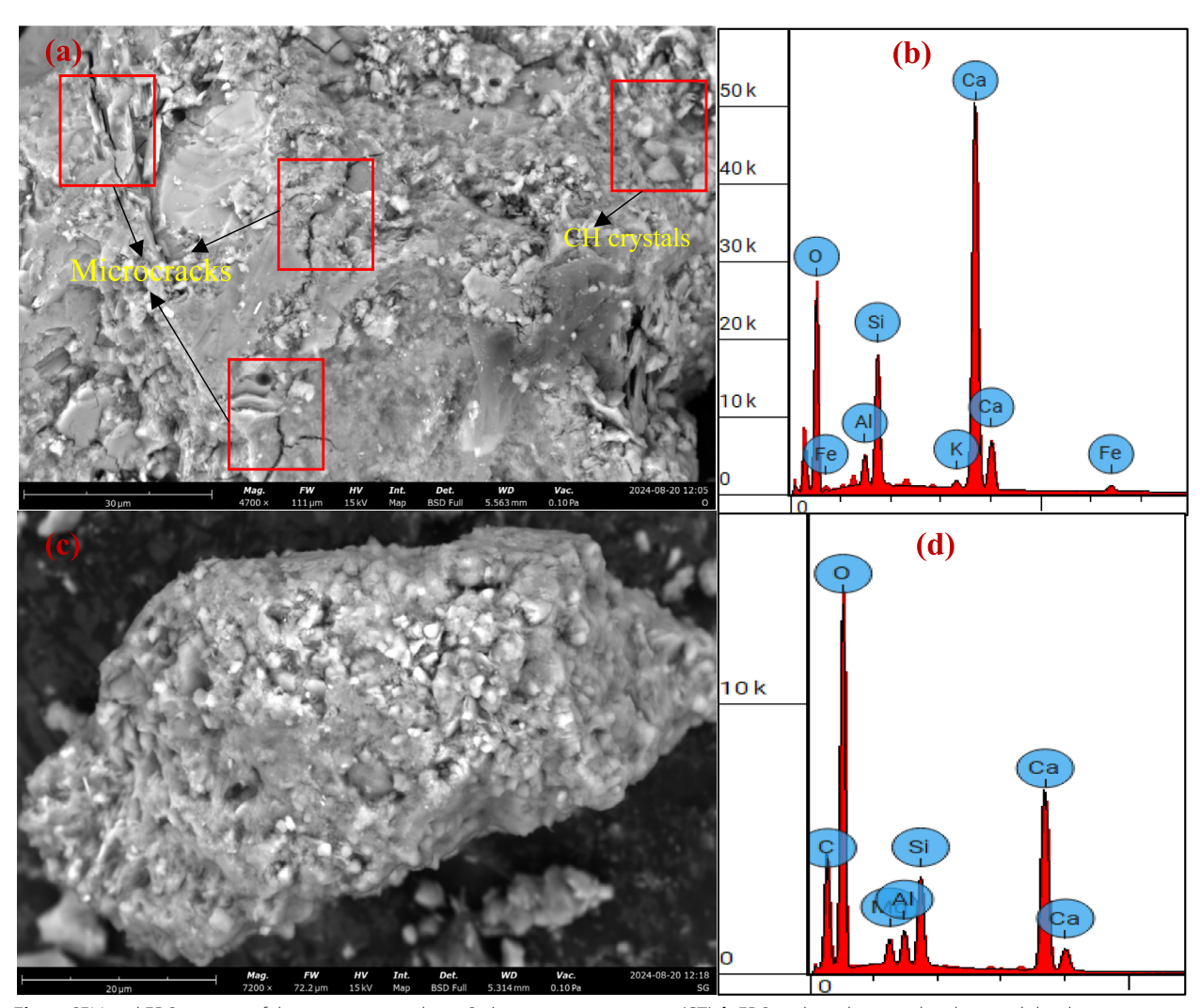


Fig. 7 SEM and EDS imagery of the concrete samples. a Ordinary cement concrete (CT). b EDS analysis showing the elemental distribution of the CT sample. c SEM image of SF and GGBS blended cement concrete sample (SF+GGBS), d EDS analysis showing the elemental distribution of the SF+GGBS sample

as described in Sect. 3.2. Free chlorides are defined as chloride ions in the cement paste matrix that are neither physically nor chemically bound to the concrete. The free chloride ion contents, which averaged over three samples per sample type are displayed in Table 7.

The results show the significant reduction of the free chloride content in the SF and SF+GGBS samples when compared to the CT sample regardless of exposure conditions. In Fig. 8, the effects of SF and GGBS on free chloride ion concentration over depth are examined by comparing graphically the SF and SF+GGBS samples with the CT sample at all three exposure conditions. Adding SF alone in the SF sample led to decrease in free chlorides through the depth of concrete compared with the CT sample. A further reduction of free chlorides in

the SF+GGBS sample is observed with the addition of GGBS under all exposure conditions. Under the IT50 condition, a relatively smaller amount of decrease in free chlorides for the SF+GGBS sample was obtained for the IT22 and IT50 conditions. Notice that the reduction of free chlorides with the addition of SF and GGBS confirms the decrease of the total chloride concentration in Fig. 6. The levels of free chlorides of the SF and SF+GGBS samples under the TG condition became close to those of the CT sample under the IT50 and IT22 conditions, respectively. Moreover, the addition of SF and GGBS under the IT50 condition lowered the free chloride content to the level of free chloride ion concentration of the CT sample under the IT22 condition.

Shittu et al. Int J Concr Struct Mater (2025) 19:54 Page 11 of 19

Table 7 Average free chloride ion content (wt.%) for the CT, SF, and SF + GGBS samples exposed to IT22, IT50, and TG conditions for 30
days

Depth (mm)	СТ			SF			SF + GGBS	SF+GGBS		
	IT22	IT50	TG	IT22	IT50	TG	IT22	IT50	TG	
10	0.2808	0.5136	0.8598	0.1804	0.2447	0.5564	0.1476	0.2209	0.4756	
20	0.1977	0.4761	0.7302	0.0687	0.1813	0.4414	0.0347	0.1778	0.3180	
30	0.1245	0.2798	0.6184	0.0335	0.1603	0.3746	0.0277	0.1416	0.2494	
40	0.0853	0.2266	0.4279	0.0121	0.0410	0.2639	0.0000	0.0250	0.1859	
50	0.0601	0.1927	0.3645	0.0000	0.0185	0.2014	0.0000	0.0151	0.1427	
60	0.0308	0.1722	0.2873	0.0000	0.0115	0.1542	0.0000	0.0100	0.1010	

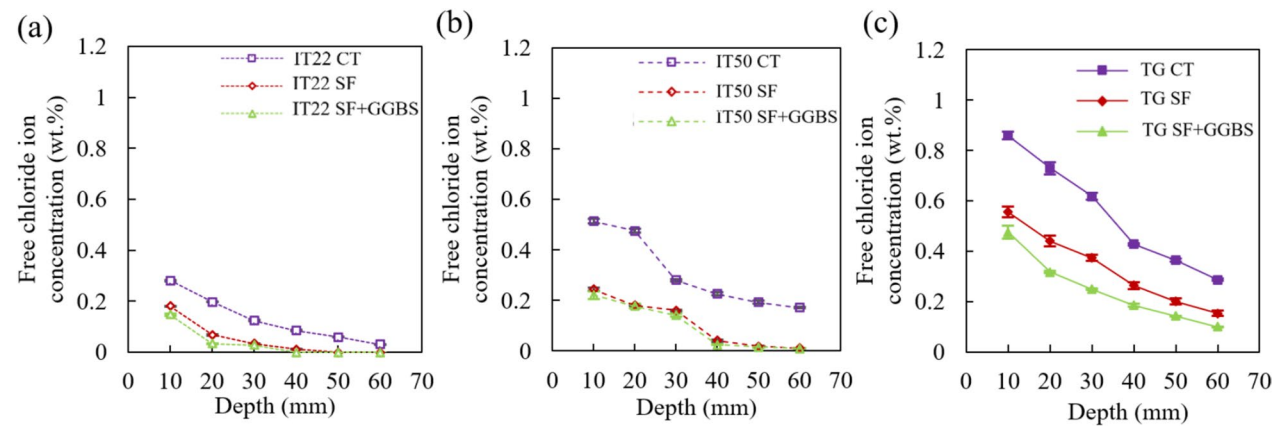


Fig. 8 Effects of SF and GGBS on free chloride ion concentration under a IT22, b IT50, and cTG exposure conditions

In Fig. 9, the influence of temperature and temperature gradient on free chloride concentration of the CT, SF, and SF+GGBS samples is investigated. From the results, it was observed that the free chloride content in concrete increases with increased temperature and much more significantly with temperature gradient. This indicates considerable increase of the total chloride concentration at high ambient temperature of 50 °C and the temperature gradient condition in Fig. 5. Under the IT22 exposure condition, there could be 36%-73% and 47%-82% decrease in the free chloride content in the SF and SF+GGBS samples, respectively, compared to the CT sample. In addition, for the IT50 condition, these reductions could be 43%-93% and 49%-94%, respectively while at the TG condition, the reduction in free chloride in the SF and SF+GGBS samples compared to the CT sample could be 35%–46%, and 45%–65%, respectively.

4.4 Chloride Binding Capacity of Concrete

The chloride binding capacity of concrete is computed by the relation between bound chloride C_b and free chloride

 C_f given by the Langmuir Isotherm in the following equation:

$$C_b = \frac{\alpha C_f}{1 + \beta C_f} \tag{3}$$

for constants α and β (Glass & Buenfeld, 2000). Although alternative isotherms such as Freundlich, linear, tri-linear, and Temkin could have been employed, the Langmuir isotherm was chosen for its ease in parameter estimation and interpretation of experimental findings in this study. In addition, by adopting the Langmuir isotherm, concrete is regarded as a homogeneous material, thereby eliminating the presence of heterogeneity-related complexities. The bound chloride is calculated by subtracting free chloride from total chloride. By fitting the free chloride content in Table 3 and the bound chloride to Eq. (3), the relations between bound and free chlorides for the CT, SF, and SF+GGBS samples were obtained for all three exposure conditions as shown in Table 8.

For better analysis of these results, the boundfree chloride relations in Table 8 are graphically displayed in Figs. 10 and 11. Figure 10 shows the effects of Shittu et al. Int J Concr Struct Mater (2025) 19:54 Page 12 of 19

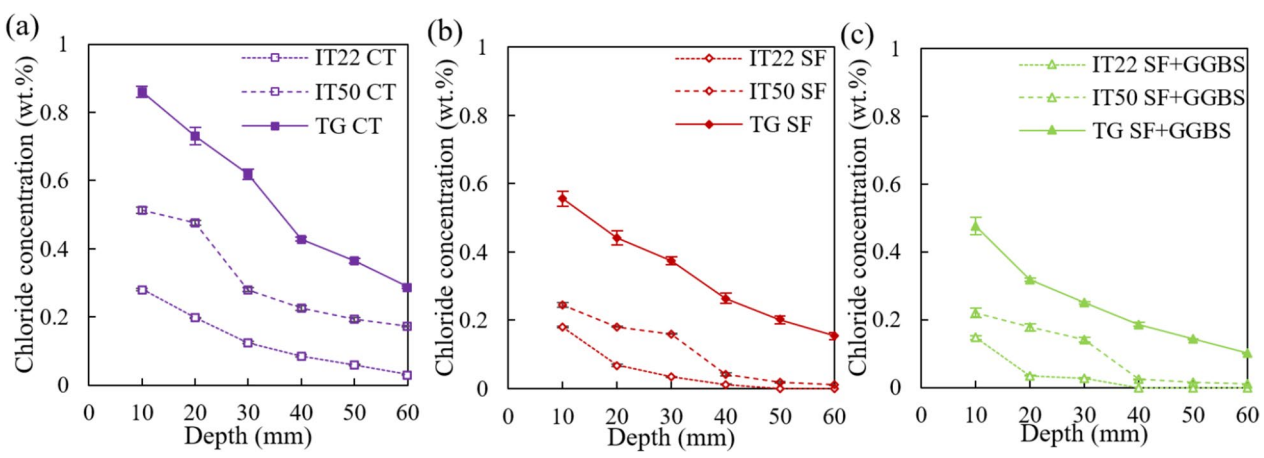


Fig. 9 Effects of temperature and temperature gradient on free chloride ion concentration: **a** CT, **b** SF, and **c** SF + GGBS samples under the IT22, IT50, and TG conditions

Table 8 Relations between bound chloride and free chloride for the CT, SF, and SF + GGBS samples under IT22, IT50, and TG conditions

Exposure condition	СТ	SF	SF + GGBS
IT22	$C_b = \frac{1.036C_f}{1 + 0.8846C_f}$	$C_b = \frac{3.245C_f}{1 + 0.5549C_f}$	$C_b = \frac{2.217C_f}{1+0.051C_f}$
IT50	$C_b = \frac{0.901C_f}{1 + 0.736C_f}$	$C_b = \frac{1.192C_f}{1 - 1.313C_f}$	$C_b = \frac{1.287C_f}{1-1.0006C_f}$
TG	$C_b = \frac{0.3549C_f}{1 + 0.8434C_f}$	$C_b = \frac{0.6146C_f}{1 + 0.09374C_f}$	$C_b = \frac{0.7677C_f}{1 + 0.1765C_f}$

temperature and temperature gradient on chloride binding capacity. These results show that high ambient temperature and temperature gradient significantly impact the ability of concrete to bind chlorides. The chloride binding capacity for all three sample sets decreases with the temperature increase from 22 to 50 °C. Temperature

rise leads to a corresponding increase in the rate of chemical reaction—chloride ion diffusion in this case. In addition, due to the increase in the overall temperature induced kinetic energy, the chloride ions are more mobile thereby limiting the ability of concrete to bind them. Furthermore, the chloride ion binding capacity is also reduced further when concrete is exposed to the TG condition as compared to the IT50 condition.

This is because, in addition to influencing the rate of chemical reaction in concrete, temperature gradient leads to variation in temperature across the concrete depth which aids chloride ion mobility and inhibits chloride ion binding in concrete.

In Fig. 11, the effects of SF and GGBS on the chloride binding capacity at the different exposure conditions are presented. Compared with the CT samples, the trend shows the increase of the chloride binding capacity with the addition of SF and GGBS for all three exposure

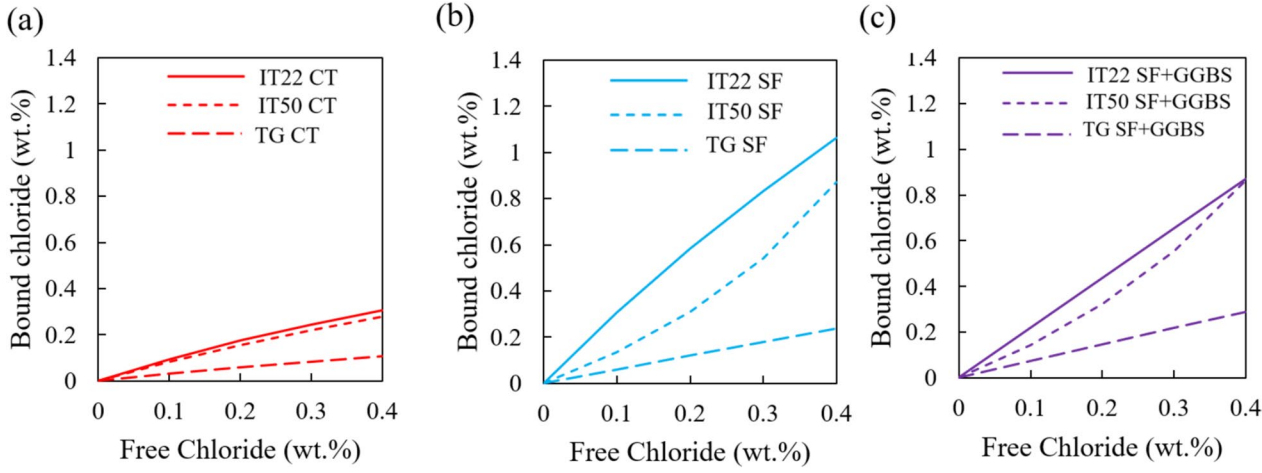


Fig. 10 Effects of temperature and temperature gradient on chloride binding capacity for a CT, b SF, and c SF + GGBS samples

Shittu et al. Int J Concr Struct Mater (2025) 19:54 Page 13 of 19

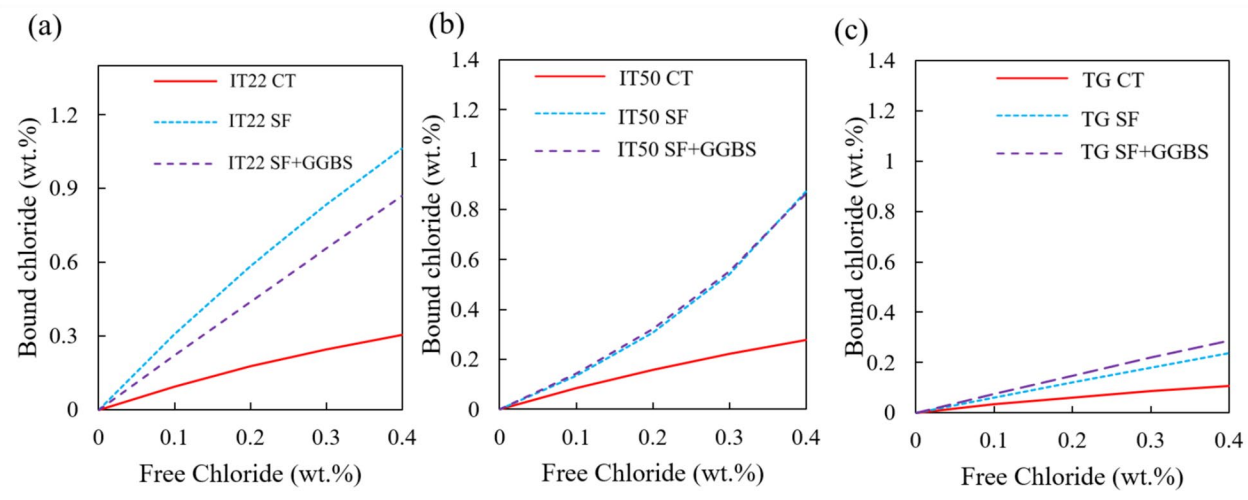


Fig. 11 Effects of SF and GGBS on chloride binding capacity of concrete samples under a IT22, b IT50, and cTG exposure conditions

conditions, indicating the reduction of the total chloride concentration in Fig. 6. This increase is less in the IT50 condition and least in the TG condition. The increase of the chloride binding capacity under the TG condition is relatively smaller than the IT22 and IT50 conditions. In addition, the binding capacity for the SF+GGBS samples is larger than that for the SF samples under the TG condition, and vice versa under the IT22 condition. On the other hand, the binding capacity for the SF and SF+GGBS samples is almost indistinguishable at the IT50 condition. Apparently, SF and GGBS are not only able to reduce the total and free chloride content but are effective in binding chlorides in concrete.

Summarily, from Figs. 10 and 11, it can be concluded that SF and GGBS are not only effective in reducing the total chloride content, as shown in Fig. 6, but they also enhance the binding capacity of concrete. According to some researchers (Hu et al., 2018), free chlorides are responsible for corrosion initiation in reinforced concrete. This implies that the inclusion of SF and GGBS can increase the corrosion initiation time in concrete. They do so by a combination of mechanisms, such as refining the pores of the concrete, blocking the path of chloride transport, reducing permeability, acting as pozzolans to improve chemical resistance of the mortar matrix, and increase the alkalinity of the concrete medium (Ahmad et al., 2022).

4.5 Effect of High Temperature and TG on Concrete Microstructure

Using SEM technique, the microstructure of the SF+GGBS samples were investigated for the three

exposure conditions—IT22, IT50, and TG, as shown in Fig. 12.

In Fig. 12a, concrete exposed to the IT22 condition exhibits a few microcracks and small pores, with no observable leaching of the C-S-H layer. In contrast, Fig. 12b shows that concrete exposed to the IT50 condition develops deeper and more dispersed pores due to the increased temperature. In Fig. 12c, concrete subjected to the TG condition has the deepest pores, along with leaching of the C-S-H layer, caused by temperature gradient effects. The largest pores formed in samples exposed to TG conditions may have been enhanced by humidity variations causing differential hydration through the concrete depth. In IT22 and IT50 exposure conditions, samples were fully cured in chloride solution at 22 and 50 °C, respectively. However, in TG exposure, only the bottom of the sample was in contact with the heated chloride solution. Therefore, in addition to accelerating chloride penetration kinetics, increased temperature and TG notably alter the concrete's microstructure, forming additional pathways for chloride ingress. These microstructural changes contribute to the increased chloride penetration in the IT50 and TG exposure condition.

5 Numerical Estimation of Chloride Concentration

In this section, chloride ion penetration into the CT, SF, and SF+GGBS samples under the temperature gradient condition is numerically estimated and validated by comparing with experimental data. To include the effects of the spatial variation of temperature and temperature gradient, we employ the modified chloride diffusion equation on domain $\Omega = [0, L]$, along with initial and boundary conditions, given by

Shittu et al. Int J Concr Struct Mater (2025) 19:54 Page 14 of 19

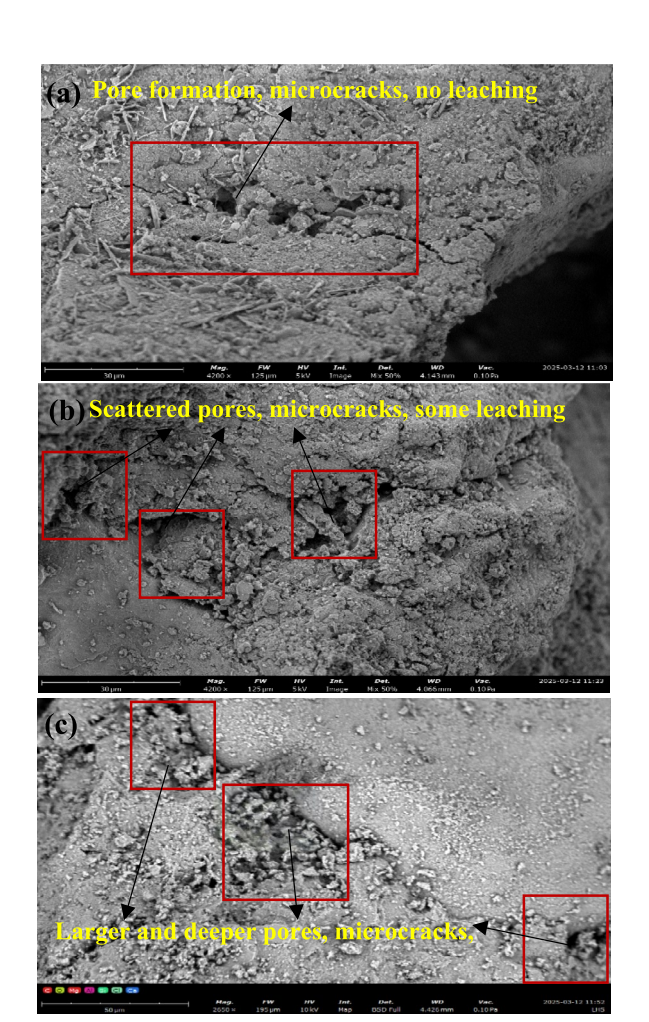


Fig. 12 SEM images showing the effect of high temperature on the microstructure of concrete samples exposed to chloride environment. **a** SF+GGBS samples exposed to room temperature of 22 °C, **b** SF+GGBS samples exposed to isothermal temperature of 50 °C, and **c** SF+GGBS samples exposed to temperature gradient condition. The pulverized samples taken from the 20 mm depth of each concrete specimen were used for the SEM analysis

contrast to the conventional diffusion equation, Eq. (4) includes the mass-diffusion coefficient $D_{Cl}(x)$ to account for the effect of the spatial (or depth) dependence of mass-diffusion in temperature and the thermo-diffusion coefficient D_T to include the effect of temperature gradient. Equation (4) reduces to the conventional diffusion equation by neglecting thermo-diffusion and the spatial dependence of $D_{Cl}(x)$.

The mass-diffusion coefficient $D_{Cl}(x)$ is estimated by the modified Arrhenius equation given by

$$D_{CI}(x) = D_0 e^{-\frac{E_a}{RT(x)}} \tag{5}$$

where R is the real gas constant (8.314 J/K mol), D_0 is the maximum diffusion coefficient, and E_a is the activation energy. Unlike the conventional Arrhenius equation, Eq. (5) includes the spatial dependent temperature T(x) to account for the spatial variation of $D_{Cl}(x)$ over the depth of concrete and reduces to the following conventional Arrhenius equation by setting T(x) = T with T being a constant, that is

$$D_{CI}(T) = D_0 e^{-\frac{E_a}{RT}}. (6)$$

To estimate the $D_{Cl}(x)$, we first evaluated the temperature-dependent mass diffusion equation $D_{Cl}(T)$ by fitting the experimental IT22 and IT50 conditions in Table 2 to the solution of the conventional diffusion equation given by

$$C(x,t) = C_s \left(1 - \operatorname{erf}\left(\frac{x}{2\sqrt{D_{Cl}t}}\right) \right) \tag{7}$$

where C_s and t represent surface chloride concentration (wt.%) and time (days), respectively, and erf is the Gaussian error function. The C_s 's for the CT, SF, and SF+GGBS samples were calculated using the same approach in our previous work (An et al., 2022). Then, substituting $D_{Cl}(T)$ at 22 and 50 °C into Eq. (6) results in two equations with two unknowns of D_0 and E_a . The two parameters D_0 and E_a are obtained by solving these two equations simulta-

$$\frac{\partial C(x,t)}{\partial t} = \nabla (D_{Cl}(x)\nabla C(x,t)) + D_T \nabla T \nabla C(x,t) \text{ on } \Omega,$$

$$C(x,0) = C_0, C(0,t) = C_s, C(L,t) = C_L$$
(4)

for chloride ion concentration C(x,t) (wt.%) at time t and depth x and temperature T (K). Here, ∇ denotes the derivative with respect to x. Equation (4) can be derived by incorporating the modified molar flux $J(x,t) = -D_{CI}(x)\nabla C - D_TC(x,t)\nabla T$ into Fick's second law as shown in our previous work (An et al., 2022). Notice that we neglect the time-dependence of temperature because there is no significant change in temperature after reaching a steady state as shown in Fig. 4a. In

neously. Eventually, $D_{Cl}(x)$ can be obtained by substituting D_0 and E_a into Eq. (5) along with T(x) in Fig. 4b. Finally, the thermo-diffusion coefficients D_T for all three samples were then estimated by fitting Eq. (4) to experimental results at the TG condition. For the CT, SF, and SF+GGBS samples, the estimated thermo-diffusion coefficient D_T and the parameters used to obtain D_T and $D_{Cl}(x)$ are reported in Table 9. Notice that the results in

Shittu et al. Int J Concr Struct Mater (2025) 19:54 Page 15 of 19

Table 9 are an average of three samples for each sample type.

The considerable increase in total chloride concentration at IT50 in Fig. 5 is confirmed by the rise in the mass diffusion coefficient $D_{Cl}(T)$ from IT22 to IT50 in Table 9. This is due to the increase of the overall thermal energy in concrete which enhances the mobility of ions with rising temperature. The mass diffusion coefficient is largely decreased with the addition of SF and GGBS that are consistent with the reduction in chloride concentration in Fig. 6. This is mainly due to the decrease of porosity with SF and SF+GGBS as shown in Table 2. Lower values of D_0 and E_a in the SF and SF+GGBS samples than the CT sample also indicate the reduction of $D_{CI}(T)$ with the addition of SF and GGBS. Notice that the reduction of $D_{Cl}(T)$ can be computed by substituting D_0 and E_a into Eq. (6). Figure 13 shows the variation of $D_{Cl}(x)$ over the depth of concrete under the TG condition obtained using the modified Arrhenius equation in Eq. (5) along with $D_{CI}(T)$ under the IT50 condition for comparison. Notice that $D_{Cl}(T)$ is constant over the depth. The results clearly show the reduction of $D_{Cl}(x)$ by including SF and its further decrease with SF+GGBS when compared to the CT sample. These results are one of the main reasons for the reduction of chloride concentration in SF and SF+GGBS in Fig. 6. Interestingly, while the decrease in $D_{Cl}(x)$ throughout the depth is prominent in the CT sample, it is minimal in the samples containing SF and GGBS. Moreover, there is no significant difference between $D_{Cl}(x)$ and $D_{Cl}(T)$ for the SF and SF+GGBS samples. Meanwhile, the SF+GGBS sample exhibited the lowest thermo-diffusion coefficient (D_T) compared to the SF and CT samples, even though the CT sample had a lower D_T value than the SF sample. However, it is important to note that this does not necessarily result in smaller chloride concentration or a longer corrosion initiation time for the CT samples, as shown in Figs. 14 and 15.

By substituting $D_{Cl}(x)$ from Fig. 13 and D_T in Table 9, chloride ion concentration over the depth of concrete was numerically estimated using the modified chloride diffusion equation in Eq. (4). Equation (4) was solved by the finite element method using MATLAB on $\Omega = [0,1]$ m and t = [0,30] days by setting $C_0 = 0$ for the initial condition and $C_L = 1$ and C_s from Table 6 for boundary conditions. In Fig. 14, chloride concentrations

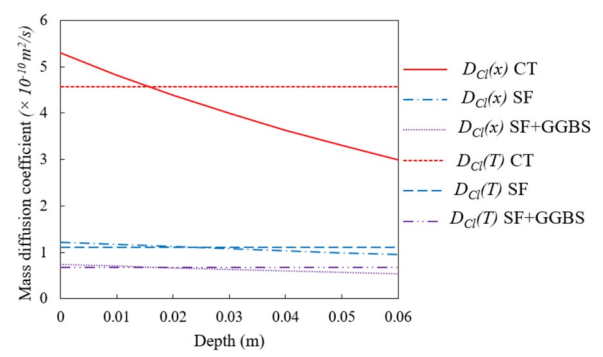


Fig. 13 Mass diffusion coefficients $D_{CI}(x)$ at the TG condition and $D_{CI}(T)$ at the IT50 condition for the CT, SF, and SF + GGBS samples

obtained numerically under the TG condition are compared with those from the experiments for all three sample types. We also provide numerical results for the IT50 condition for comparison. To study the effect of the temperature gradient, numerical simulations were performed for two cases. One is to solve Eq. (4) by considering only mass diffusion without thermo-diffusion, i.e., $D_{CI}(x)$ only, and the other is to solve it with both mass- and thermodiffusion, i.e., $D_{Cl}(x)$ and D_T . For all three types of samples, neither the chloride concentrations obtained using $D_{Cl}(x)$ only nor $D_{Cl}(T)$ represented the experimental results under the TG condition. However, the experimental results are close to the numerical ones obtained by considering both mass- and thermo-diffusion, i.e., $D_{Cl}(x)$ and D_T , in Eq. (4). These results verify the importance of temperature gradient on chloride diffusion in concrete structures, in addition to chloride ion concentration gradient and temperature.

Equation (4) was applied to estimate the corrosion initiation time of a RCB in nuclear power plants. In this study, we consider a RCB in an APR1400 nuclear power plant with a rebar depth of 20 cm embedded in a 1.47 m thick wall (An et al., 2022). The temperature values (22 and 50 °C) employed in the experimental setup and adopted for the numerical analysis aligns with conditions typical of the RCB located in the Arabian Gulf. A maximum external temperature of 50 °C corresponds to peak summer conditions, while an internal temperature of 22 °C

Table 9 Estimated mass diffusion coefficient $D_{CI}(T)$ and thermo-diffusion coefficient D_T for CT, SF, and SF + GGBS samples and the parameters C_S , D_0 , and E_a used for the estimation of $D_{CI}(T)$, $D_{CI}(x)$, and D_T

Sample Type	C _s (wt.%)	$D_0(\mathrm{m}^2/\mathrm{s})$	$E_a(J/mol)$	$D_T (\times 10^{-11} \mathrm{m}^2 / \mathrm{sK})$	$D_{CI}(T) \times 10^{-11} \text{m}$	n ² /s
					22 °C(IT22)	50 °C(IT50)
CT	1.059	1.39 × 10 ¹	64,821	8.30	4.63	45.64
SF	0.926	4.43×10^{-4}	40,803	13.00	2.64	11.16
SF+GGBS	0.853	1.12×10^{-5}	32,215	7.90	2.18	6.81

Shittu et al. Int J Concr Struct Mater (2025) 19:54 Page 16 of 19

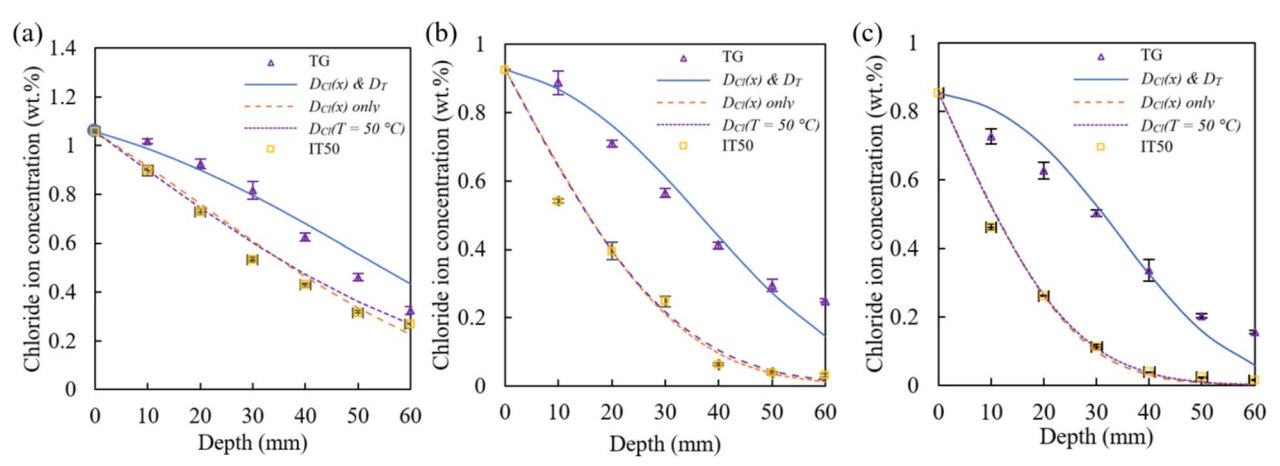


Fig. 14 Numerical estimation of chloride concentration for **a** CT, **b** SF, and **c** SF + GGBS samples under the TG condition. Both numerical and experimental results under the IT50 and TG conditions are displayed for validation and comparison. TG (triangle) and IT50 (square) are experimental results. The solid, dashed, and dotted lines represent the numerical results obtained from Eq. (4) by only considering $D_{CI}(x)$ and $D_{T}(x)$ only, and $D_{CI}(T)$, respectively

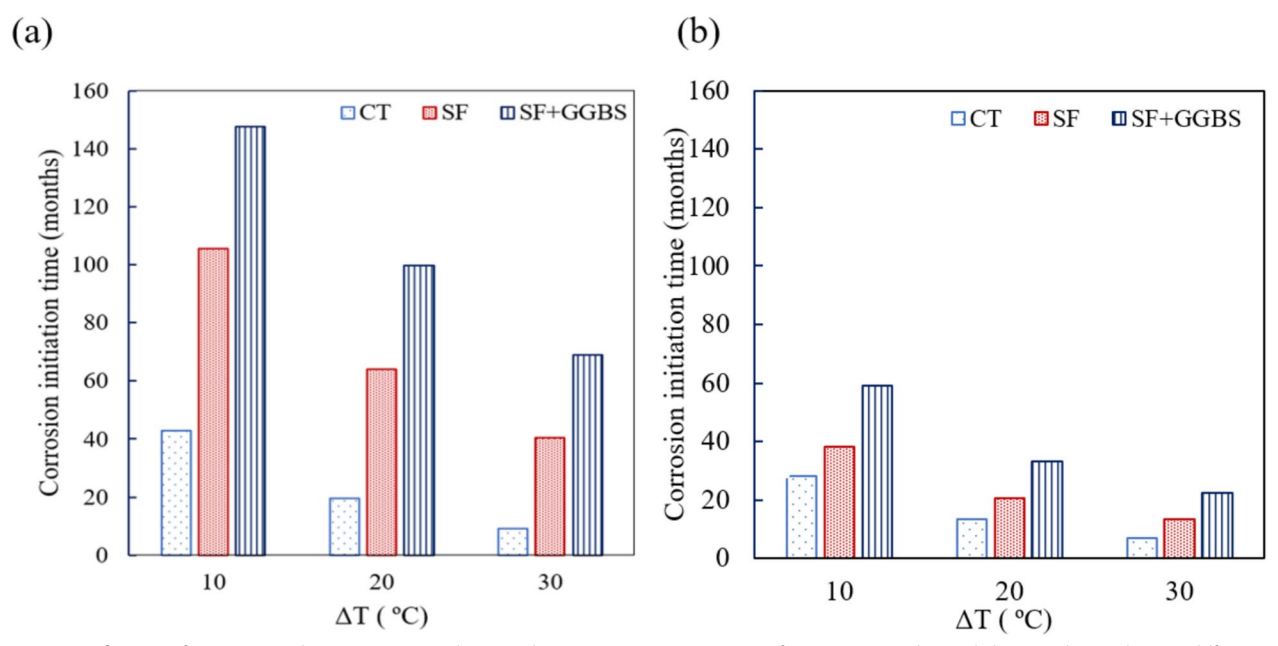


Fig. 15 Influence of SF, GGBS, and temperature gradient on the corrosion initiation time of an RCB situated in arid climate when **a** thermo-diffusion is neglected and **b** when thermo-diffusion is considered at ΔT / wall thickness

reflects standard operating conditions within the RCB. Despite the substantial heat generated by the nuclear reaction, potentially leading to temperatures reaching hundreds of degrees Celsius, the APR 1400 utilizes pressurized water as both coolant and moderator (Emirates Nuclear Energy Corporation, 2023). Control over internal temperature is crucial for preserving the structural integrity of the RCB and other components housed within the containment building (Alameri et al., 2020). Also, we set

chloride threshold, defined as the minimum chloride ion content at rebar depth to initiate corrosion, of 1 wt.% of binder (Vijayan et al., 2023) which is equivalent to 0.1685 (wt. %) of concrete. Equation (4) was solved numerically using $D_{Cl}(x)$ in Fig. 12 and D_T in Table 6 by setting $C_0=0$ for the initial condition and $C_L=5$ and C_s from Table 6 for boundary conditions. The corrosion initiation time, corresponding to chloride concentration of 0.1685 (wt. %) at 20 cm depth, is estimated at three temperature

Shittu et al. Int J Concr Struct Mater (2025) 19:54 Page 17 of 19

gradients, i.e., $\Delta T = 10^{\circ}$ C, 20° C, and 30° C, for different scenarios that either consider or ignore thermo-diffusion to study the effect of temperature gradient. It is important to note that this numerical model is applicable only within ambient temperature ranges, where the salt medium does not undergo phase changes. This means that freezing, boiling, and evaporation phenomena are not accounted for in the model.

The corrosion initiation times for the CT, SF, and SF+GGBS samples are presented as a function of temperature gradient in Fig. 15. Figure 15a shows the corrosion initiation time for $D_{CI}(x)$ only, i.e., only mass diffusion without thermo-diffusion. Figure 15b shows the corrosion initiation time for $D_{CI}(x)$ and D_T , i.e., a coupled mass- and thermo-diffusion. An increase in temperature gradient yielded a significant decrease in the time to initiation of corrosion in all the concrete samples in Fig. 15a, b. A further reduction of corrosion initiation time was obtained by considering thermo-diffusion in Fig. 15b, showing the importance of thermal diffusion in the service life prediction of concrete structures at high ambient temperature. Moreover, the addition of SF and GGBS resulted in increasing corrosion initiation time indicating the longer service life of the RCB. Therefore, stakeholders in the construction industry, especially in arid regions, must consider the influence of thermodiffusion on the ingress of chemical agents into concrete. This is particularly crucial for critical concrete structures, such as dams, nuclear power plants (NPPs), and bridges, which are exposed to both thermal and chloride concentration gradients. To enhance concrete performance, materials with low thermal diffusivity, such as specific aggregates, should be prioritized. In addition, using lowheat cement, like Type IV Portland cement, can minimize heat generation during hydration (Fang et al., 2025; Ma et al., 2024). The incorporation of pozzolans—such as SF, GGBS, and fly ash—can further reduce heat production. Reflective coatings and surface treatments can also help reduce heat absorption by concrete. Furthermore, design standards should be updated to require thermal diffusivity testing for aggregates, binders, and concrete mixes in arid climates. It is also advisable to promote climatespecific thermal modeling of concrete structures. Finally, post-construction monitoring protocols in arid environments should include thermal diffusivity inspections, and service life prediction models should account for accelerated chloride penetration due to thermo-diffusion in concrete structures located in hot, humid regions of arid climates.

Notice that the corrosion initiation time in this study was estimated using parameters calibrated with experimental data for fully saturated concrete condition.

Consequently, these estimated times could be higher than in real life. However, this study verifies the possibility of applying the modified chloride diffusion equation in Eq. (4) for the service life prediction of concrete structures based on the corrosion initiation time in arid climates.

6 Conclusion

The influence of SF and GGBS on chloride ion penetration into concrete at high ambient temperature of 50 °C in arid climate (e.g., MENA region) was investigated. To achieve this, the CT samples containing only cement as a binder were compared with the SF samples including cement and SF and the SF + GGBS samples with a combination of cement, SF, and GGBS. These samples were either totally or partially immersed in saturated NaCl to simulate isothermal (IT22 and IT50) and temperature gradient (TG) exposure conditions. The total and free chloride concentrations through the depth of the concrete samples exposed to three different exposure conditions were measured via potentiometric titration. The key findings from the study are summarized:

- The chloride concentration in samples exposed temperature gradient (TG) condition could be 1.3–6 times higher than the equivalent isothermal condition.
- Under the TG condition, the inclusion of SF, and SF with GGBS at the proportion demonstrated in this study can reduce the chloride concentration by up to 13%–93%, and 29%–95%, respectively.
- Adding SF and GGBS to concrete samples as used in this work improved the chloride binding capacity of the concrete samples for all exposure conditions.
- Thermal diffusion accelerates chloride penetration into concrete, while it significantly diminishes the chloride binding capacity of concrete.
- Using SEM technique, there appears to be larger pores in the samples exposed to TG condition when compared to the two other exposure conditions
- The corrosion initiation time could be reduced by up to 62% due to thermal diffusion. Although there could be 36% and 109% increase in these values for samples containing SF, and SF with GGBS, respectively under the TG condition when compared to the control samples.

Most of the findings of this study were obtained using chemical analysis in the laboratory. More so, the concrete samples under the TG condition were exposed to chloride environment in saturated conditions reducing Shittu et al. Int J Concr Struct Mater (2025) 19:54 Page 18 of 19

the effect of humidity gradient. A real-life scenario involves the combined impact of thermal and humidity gradients. In addition, the effects of long-term exposure of concrete samples to chloride solution under the influence of thermal diffusion need to be investigated. A particular constraint in the experiment is setting up the TG condition. Only a few samples can be tested at a particular duration, because, for larger amounts of samples, the evaporation rate becomes uncontrollable, leading to fluctuations in the NaCl solution concentration over time. In future studies, a smaller sample size will be used to accommodate a large number of samples in a water bath. In addition, the samples will be exposed to longer than 30 days to examine the impact of long-term exposure on thermal diffusion in concrete.

Abbreviations

SF Silica fume

GGBS Ground granulated blast furnace slag

FA Fly ash

C–A–H Calcium–aluminate–hydrate
C–S–H Calcium–silicate–hydrate
RCB Reactor containment building
XRD X-ray powder diffraction

JCPDS Joint committee on powder diffraction standards

LOI Loss on ignition NaCl Sodium chloride CT Control sample

IT22 Isothermal condition at 22 °C IT50 Isothermal condition at 50 °C TG Temperature gradient condition

 C_b Bound chloride C_f Free chloride

 $D_{CI}(T)$ Temperature-dependent chloride diffusion coefficient

 $D_{CI}(x)$ Spatial chloride diffusion coefficient D_T Thermo-diffusion coefficient E_a Activation energy SEM Scanning electron microscopy

SEM Scanning electron microscopy
EDS Energy dispersive spectroscopy

Acknowledgements

The research was carried out by the Emirates Nuclear Technology Center, a collaboration amongst Khalifa University of Science and Technology, Emirates Nuclear Energy Corporation and the Federal Authority for Nuclear Regulation.

Author contributions

RAS: Methodology, visualization, analysis, writing—original draft, revision, and editing final draft. AA: Funding and editing final draft. AKA: Funding and editing final draft. TYK: Conceptualization, funding, supervision, methodology, original draft and editing final draft.

Availability of data and materials

This manuscript has no associated data

Declarations

Competing interests

The authors declare that they have no known competing financial interests or personal relationships that could have appeared to influence the work reported in this paper.

Received: 8 October 2024 Accepted: 15 April 2025 Published online: 03 July 2025

References

- Ahmad, J., Kontoleon, K. J., Majdi, A., Naqash, M. T., Deifalla, A. F., Ben Kahla, N., & Qaidi, S. M. (2022). A comprehensive review on the ground granulated blast furnace slag (GGBS) in concrete production. *Sustainability*, *14*(14), 8783. https://doi.org/10.3390/su14148783
- Alameri, S. A., & Alkaabi, A. K. (2020). Fundamentals of nuclear reactors. In S. Khan & A. Nakhabov (Eds.), *Nuclear reactor technology development and utilization* (pp. 27–60). Elsevier.
- Al-Sodani, K. A. A., Al-Zahrani, M. M., Maslehuddin, M., Al-Amoudi, O. S. B., & Al-Dulaijan, S. U. (2021). Chloride diffusion models for Type I and fly ash cement concrete exposed to field and laboratory conditions. *Marine* Structures, 76, 102900. https://doi.org/10.1016/j.marstruc.2020.102900
- Al-Sodani, K. A. A. (2022). Effect of exposure temperatures on chloride penetration resistance of concrete incorporating polypropylene Fibers, silica fume and metakaolin. *Construction and Building Materials*, 346, 128445. https://doi.org/10.1016/j.conbuildmat.2022.128445.
- An, B., Cho, P., Shittu, R. A., Kim, T. Y., Rostron, P., AlFantazi, A., & Yi, Y. (2022). Effect of temperature gradient on chloride ion diffusion in nuclear reactor containment building concrete. *Energies*, *15*(15), 5581. https://doi.org/10.3390/en15155581
- Arivalagan, S. (2014). Sustainable studies on concrete with GGBS as a replacement material in cement. *Jordan Journal of Civil Engineering*, 8(3), 263–270.
- ASTM. (2012a). C1152/C1152M-04(2012)e1, Standard test method for acid-soluble chloride in mortar and concrete. ASTM International.
- ASTM. (2012b). C1218/C1218M-17(2012)e1, Standard test method for water-soluble chloride in mortar and concrete. ASTM International.
- ASTMC642-06. (2006). C 642-06: Standard test method for density, absorption, and voids in hardened concrete. *ASTM Int*. pp. 11–13.
- Bai, Y., Wang, Y., & Xi, Y. (2020). Modeling the effect of temperature gradient on moisture and ionic transport in concrete. *Cement and Concrete Composites*, 106, 103454. https://doi.org/10.1016/j.cemconcomp.2019.103454
- Basha, B. G., Rao, B. K., & Rao, C. H. (2020). Service life prediction of R.C structure incorporated with GGBS & silica fume subjected to chloride ion penetration. *Materials and Today Proceedings*, 33, 245–252. https://doi.org/10.1016/j.matpr.2020.04.040
- Bolzoni, F., Brenna, A., & Ormellese, M. (2022). Recent advances in the use of inhibitors to prevent chloride-induced corrosion in reinforced concrete. *Cement and Concrete Research*, 154, 106719. https://doi.org/10.1016/j.cemconres.2022.106719
- Emirates Nuclear Energy Corporation. (2023). APR1400: Advanced Technology.

 Accessed April 18, 2023. https://www.enec.gov.ae/barakah-plant/technology/
- Criado, M., Bernal, S. A., Garcia-Triñanes, P., & Provis, J. L. (2018). Influence of slag composition on the stability of steel in alkali-activated cementitious materials. *Journal of Materials Science*, *53*(7), 5016–5035. https://doi.org/10.1007/s10853-017-1919-3
- de Assis Oliveira, J., Ribeiro, J. C. L., Pedroti, L. G., & Nalon, G. H. (2024). Effects of different cooling methods on the resistance to chloride ion penetration in concrete produced with slag-modified cement and exposed to elevated temperatures. *Journal of Building Engineering*, *91*, 109488. https://doi.org/10.1016/j.jobe.2024.109488
- Dehwah, O. H., & Xi, Y. (2024). Theoretical model for the coupling effect of moisture transport on chloride penetration in concrete. *Cement and Concrete Research*, 177, 107431. https://doi.org/10.1016/j.cemconres.2024. 107431
- Elchalakani, M., Aly, T., & Abu-Aisheh, E. (2014). Sustainable concrete with high volume GGBFS to build Masdar City in the UAE. *Case Studies in Construction Materials*, 1, 10–24. https://doi.org/10.1016/j.cscm.2013.11.001
- Fang, L., Fu, D., Yuan, Q., Xu, S., Zhang, D., Cai, H., & Zhou, J. (2025). Combined effects of low-heat cement, expansive agent and shrinkage-reducing admixture on drying shrinkage and cracking of concrete. Case Studies in Construction Materials, 22, e04344. https://doi.org/10.1016/j.cscm.2025. e04344
- Gjørv, O. E. (2011). Durability of concrete structures. *Arabian Journal for Science and Engineering*, *36*(2), 151–172. https://doi.org/10.1007/s13369-010-0033-5
- Glass, G. K., & Buenfeld, N. R. (2000). The influence of chloride binding on the chloride induced corrosion risk in reinforced concrete. *Corrosion Science*, 42(2), 329–344.
- Hu, X., Shi, C., Yuan, Q., Zhang, J., & De Schutter, G. (2018). Influences of chloride immersion on zeta potential and chloride concentration index

Shittu et al. Int J Concr Struct Mater (2025) 19:54 Page 19 of 19

- of cement-based materials. Cement and Concrete Research, 106(January), 49–56.
- Huynh, T. P., Ho, L. S., & Van Ho, Q. (2022). Experimental investigation on the performance of concrete incorporating fine dune sand and ground granulated blast-furnace slag. *Construction and Building Materials*, 347, 128512. https://doi.org/10.1016/j.conbuildmat.2022.128512
- Iqbal, M., Zhang, D., Khan, K., Amin, M. N., Ibrahim, M., & Salami, B. A. (2023). Evaluating mechanical, microstructural and durability performance of seawater sea sand concrete modified with silica fume. *Journal of Building Engineering*, 72, 106583. https://doi.org/10.1016/j.jobe.2023.106583
- Isteita, M., & Xi, Y. (2017). The effect of temperature variation on chloride penetration in concrete. *Construction and Building Materials*, 156, 73–82. https://doi.org/10.1016/j.conbuildmat.2017.08.139
- Jagan, S., & Neelakantan, T. R. (2021). Effect of silica fume on the hardened and durability properties of concrete. *International Review of Applied Sciences* and Engineering, 12(1), 44–49. https://doi.org/10.1556/1848.2020.00129
- Kumaran, M. K. (1987). Moisture transport through glass-fibre insulation in the presence of a thermal gradient. *Journal of Thermal Insulation*, *10*(4), 243–255. https://doi.org/10.1177/109719638701000405
- Luo, R., Cai, Y., Wang, C., & Huang, X. (2003). Study of chloride binding and diffusion in GGBS concrete. *Cement and Concrete Research*, 33(1), 1–7. https://doi.org/10.1016/S0008-8846(02)00712-3
- Ma, R., Bu, Y., Liu, H., Lu, C., Liu, H., & Guo, S. (2024). Low-heat & early-strength well cement system: Application of HSA in hydrate layer cementing. *Geo-energy Science and Engineering*, 241, 213169. https://doi.org/10.1016/j. geoen.2024.213169
- Nguyen, H. A., Chang, T. P., Shih, J. Y., Chen, C. T., & Nguyen, T. D. (2016). Sulfate resistance of low energy SFC no-cement mortar. Construction and Building Materials, 102(January), 239–243. https://doi.org/10.1016/j.conbu ildmat.2015.10.107
- Qin, M., & Belarbi, R. (2005). Development of an analytical method for simultaneous heat and moisture transfer in building materials utilizing transfer function method. *Journal of materials in civil engineering*, 17(5), 492–497. https://doi.org/10.1061/ASCE0899-1561200517:5492.
- Reshma, T. V., Patnaikuni, C. K., Tanu, H. M., & Bharath, A. (2023). Evaluation of strength, durability, and microstructure characteristics of slag-sandinduced concrete. *Cleaner Materials*, 10, 100212. https://doi.org/10.1016/j. clema.2023.100212.
- Shelote, K. M., Bala, A., & Gupta, S. (2023). An overview of mechanical, permeability, and thermal properties of silica fume concrete using bibliographic survey and building information modelling. *Construction and Building Materials*, 385, 131489. https://doi.org/10.1016/j.conbuildmat.2023. 131489
- Sothornchaiwit, K., Dokduea, W., Tangchirapat, W., Keawsawasvong, S., Thongchom, C., & Jaturapitakkul, C. (2022). Influences of silica fume on compressive strength and chemical resistances of high calcium fly ashbased alkali-activated mortar. *Sustainability*, *14*(5), 2652. https://doi.org/10.3390/su14052652
- Tanu, H. M., & Unnikrishnan, S. (2023). Durability and elevated temperature behaviour of geopolymer concrete developed with ground granulated blast furnace slag and sugarcane bagasse ash. *Journal of Building Pathology and Rehabilitation*, 8(2), 106. https://doi.org/10.1007/s41024-023-00354-7
- Tanu, H. M., & Unnikrishnan, S. (2023). Mechanical strength and microstructure of GGBS-SCBA based geopolymer concrete. *Journal of Materials Research* and Technology, 24, 7816–7831. https://doi.org/10.1016/j.jmrt.2023.05.051
- Tian, Y., Zhang, G., Ye, H., Zeng, Q., Zhang, Z., Tian, Z., & Wang, J. (2023). Corrosion of steel rebar in concrete induced by chloride ions under natural environments. Construction and Building Materials, 369, 130504. https://doi.org/10.1016/j.conbuildmat.2023.130504
- Vijayan, D. S., Devarajan, P., & Sivasuriyan, A. (2023). A review on eminent application and performance of nano based silica and silica fume in the cement concrete. Sustainable Energy Technologies and Assessments, 56, 103105. https://doi.org/10.1016/j.seta.2023.103105
- Zhang, J., Guo, J., Li, D., Zhang, Y., Bian, F., & Fang, Z. (2017). The influence of admixture on chloride time-varying diffusivity and microstructure of concrete by low-field NMR. *Ocean Engineering*, 142(February), 94–101. https://doi.org/10.1016/j.oceaneng.2017.06.065
- Zhao, R., Jin, Z., Feng, G., & Li, J. (2020). Chloride diffusion and induced reinforcement corrosion in concrete with fly ash and ground-granulated blast-furnace slag exposed to marine submerged zone. *Advances in*

Materials Science and Engineering, 2020(1), 8881446. https://doi.org/10. 1155/2020/8881446

Publisher's Note

Springer Nature remains neutral with regard to jurisdictional claims in published maps and institutional affiliations.

Remilekun A. Shittu Post-doctoral fellow, Emirates Nuclear Technology Center.

Akram AlFantazi Professor, Chemical Engineering, and Project lead at Emirates Nuclear Technology Center.

Ahmed K. Alkaabi Assistant Professor, Mechanical and Nuclear Engineering, and Project lead at Emirates Nuclear Technology Center.

Tae-Yeon Kim Associate Professor, Civil Infrastructure and Environment Engineering, member of Emirates Nuclear Technology Center.